Cross sections for the formation of $^{195}Hg^{m,g}$, $^{197}Hg^{m,g}$ and $^{196}Au^{m,g}$ in alpha and ^{3}He-particle induced reactions on Pt: Effect of level density parameters on the calculated isomeric cross–section ratio

S. Sudár[1,2] and S.M. Qaim[1*]

[1] *Institut für Nuklearchemie, Forschungszentrum Jülich GmbH, D-52425 Jülich, Germany and*

[2] *Institute of Experimental Physics, University of Debrecen, H-4010 Debrecen Pf. 105, Hungary.*

(Dated: February 1, 2006)

Abstract

Excitation functions were measured for the reactions ^{nat}Pt(^{3}He, xn)^{195}Hg^{m,g}, ^{nat}Pt(^{3}He, xn)^{197}Hg^{m,g}, ^{nat}Pt(^{3}He, x)^{196}Au^{m,g} and ^{nat}Pt(α, xn)^{197}Hg^{m,g} over the energy range of 18 to 35 MeV for ^{3}He-particles and 17 to 26 MeV for alpha particles. The reactions ^{197}Au(p, n)^{197}Hg^{m,g} were also investigated over the proton energy range of 6 to 20 MeV. The three projectiles were produced at the Jülich variable energy compact cyclotron (CV 28). Use was made of the activation technique in combination with conventional high-resolution as well as low-energy HPGe-detector γ-ray spectroscopy. For most of the reactions, the present measurements provide the first consistent sets of data. From the available experimental data, isomeric cross-section ratios were determined for the above mentioned reactions. Nuclear model calculations using the code STAPRE, which employs the Hauser-Feshbach (statistical model) and exciton model (precompound effects) formalisms, were undertaken to describe the formation of both the isomeric and ground states of the products. The calculations were compared with the results of the EMPIRE-II code. The excitation functions of the (^{3}He, xn) and (α, xn) processes are described well by the theory. In the case of (^{3}He, pxn) reactions, however, considerable deviations were observed between the experiment and the theory, presumably due to strong contributions from direct interactions. A description of the isomeric cross-section ratio by the model was possible only with a very low value of η, i.e. the $\Theta_{eff}/\Theta_{rig}$ ratio. A mass dependence of η is *proposed.*

PACS numbers: 24.10.-i, 24.60.Dr, 25.10.+s, 25.40.-h

*Corresponding author. E-mail: s.m.qaim@fz-juelich.de

I. INTRODUCTION

Studies of excitation functions of nuclear reactions are of considerable importance for testing nuclear models as well as for practical applications. Furthermore, isomeric cross-section ratios are of fundamental interest. It is now known that the isomeric cross-section ratio is primarily governed by the spins of the levels involved, rather than their separation energies [1, 2]. In addition, through detailed studies on the formation of $^{73}Se^{m,g}$ in six nuclear reactions [1], $^{58}Co^{m,g}$ in seven nuclear reactions [3], $^{94}Tc^{m,g}$ in three nuclear reactions [4], and $^{120}I^{m,g}$ in three nuclear processes [5], involving different combinations of target, projectile and ejectile, the effect of change in ratio of the moment of inertia to the rigid body moment of inertia, assumptions regarding the angular momentum distribution after pre-equilibrium (PE) decay, spin and parity assignments of discrete levels, branching ratios of γ-rays from discrete levels, and ratios of strengths of γ-rays of different multipole types, have been elucidated. In a model case of isomeric pairs with identical metastable and ground state spins, the influence of reaction channel on the isomeric cross-section ratio was also demonstrated [6]. All those studies were, however, limited to nuclei with mass numbers up to 120. Furthermore, the spins of the levels involved were not very high. We now extended those studies to nuclei of higher masses and levels of higher spins. Two isomeric pairs, namely $^{195}Hg^{m,g}$ and $^{197}Hg^{m,g}$ appeared to be very interesting: in both cases the ground state has a low spin ($1/2^-$) and the metastable state a higher spin ($13/2^+$). A third isomeric pair, viz. $^{196}Au^{m,g}$, with ground and metastable state spins of (2^-) and (12^-), respectively, also constitutes an interesting case. In contrast to commonly used projectiles, neutrons and protons, we decided to investigate reactions induced by ^{3}He- and alpha particles. The higher angular momentum brought by those projectiles might shed some more light on the effect of spin distribution of the level density on the isomeric cross-section ratio.

A common assumption in the global parametrization of the nuclear level density within the framework of the Fermi gas model is that the spin distribution is described by the formula

$$\frac{\rho_J}{\rho} = \frac{2J+1}{2\sqrt{2\pi}\sigma^3} e^{-\frac{J(J+1)}{2\sigma^2}} \tag{1}$$

where ρ is the total level density, while ρ_J is the density of spin-J levels without the $2J+1$ degeneracy factor. The paramter σ is known as spin-cutoff parameter. The ρ, ρ_J and σ are

all functions of the excitation energy. The spin-cutoff parameter can be expressed in terms of the expected value of the $\vec{J}^2$

$$\sigma^2 = \frac{1}{3} < \vec{J}^2 > \tag{2}$$

In thermal ensembles it is common to define an effective moment of inertia Θ_{eff} by the relation between $< \vec{J}^2 >$ and temperature T, which we can write as

$$\Theta_{eff} = \frac{\hbar^2}{T}\sigma^2 \tag{3}$$

In the empirical parametrization, the σ is determined using the rigid body moment of inertia

$$\Theta_{rig} = \frac{2}{5}mA(r_0 A^{1/3})^2, \tag{4}$$

where r_0 is the nuclear radius parameter, A the mass number and m is the nucleon mass. Introducing the $(\eta = \Theta_{eff}/\Theta_{rig})$ the square of the spin-cutoff parameter can be expressed as

$$\sigma^2 = \eta\frac{\Theta_{rig}T}{\hbar^2} \tag{5}$$

Since Bethe's pioneering work [7] the nuclear level density problem has remained an active area of both theoretical and experimental studies. The above formulas are based on the noninteracting fermion gas in the nuclear volume, having equally spaced energy levels. Such a model corresponds to the zeroeth-order approximation of a Fermi gas model. The original Bethe formula was later refined to take into account the shell and pairing effects. One of the refined formulas is the back-shifted Fermi gas (BSFG) model [8]. Recent theoretical studies are based on microscopic statistical model [9, 10] which is beginnig to approach the quality of the semiempirical models, but its results are available only in the form of numerical data. Theoretical studies have shown that the spin dependence of the level density can deviate from the simple formula given above at a high spin [11]. Studies on the spin distribution are interesting both from the theoretical [12] and experimental points of view. The theoretical analysis has also shown the excitation energy dependence of the spin-cutoff parameter [13].

The spin distribution of the levels can be studied experimentally by investigating the rotational band of the nuclei[14] or by comparing the measured and calculated isomeric cross-section ratios [1, 3–5, 15].

A literature survey [16] showed that, in general, very little information is available for high spin isomer production, for example,on the $^{195}Hg^{m,g}$, $^{197}Hg^{m,g}$ and $^{196}Au^{m,g}$ mentioned

above. A few reports exist in the literature [17–21] on the ^{197}Au(p,n)^{197}Hg^{m,g} process. The results above 10 MeV, however, are conflicting. Vandenbosch and Huizenga [17] studied the production of ^{197}Hg^{m,g} isomers in two reactions, namely, (p,n) and $(d,2n)$, and isomer cross-section ratios in (n,γ), (d,p), $(n,2n)$, $(\alpha,\alpha n)$ and (α,xn) reactions. Based on the isomeric cross-section ratio, the spin-cutoff parameter (σ) was determined and the ratio of the effective moment of inertia Θ_{eff} to the rigid-body moment of inertia $\Theta_{rig}(\eta = \Theta_{eff}/\Theta_{rig})$ was found to be about 0.1 which is in disagreement with the usual value of 0.5 for it. Some later measurements [18, 19, 21] gave higher isomeric cross-section ratios for the ^{197}Au$(p,n)^{197}$Hg^{m,g} process. For the other nuclear processes studied in this work, no cross-section data were found in the literature.

II. EXPERIMENT

Cross sections were measured by the stacked-foil technique which involves the irradiation of a set of thin foils and identification of the radioactive products. This activation method is very suitable for investigating the reaction products and is almost ideal for studying closely spaced low-lying isomeric states, provided their lifetimes are not too short. The details have been described over the years in several publications [cf. 22–25]. Here we give only some salient features relevant to the present measurements.

A. Samples and irradiations

High purity thin platinum foils (99.9%, 12.5μm, supplied by Johnson-Matthey, England) were used as samples. In a given stack about 4 or 5 such foils were placed together with Ti foils for monitoring the ^{3}He-beams and Cu foils for α-particle beams. The monitor foils also served to degrade the projectile energy as well as to determine the incident particle energy and the beam intensity. Different arrangements of the Pt and monitor foils allowed changes in the mean energies of the irradiated platinum samples. Each stack was irradiated for 30-60 minutes using the ^{3}He- and α-particle beams of intensities about 100 nA at the Compact Cyclotron CV 28 at the Forschungszentrum (FZ) Jülich. The primary energies used were 27.7 MeV for α- and 36.9 MeV for ^{3}He-particles. The energy of the particle beam was measured before or after the irradiation and had an uncertainty of 0.15 MeV [26]. A total of

TABLE I: A typical stack composition for alpha particle induced reaction on Pt

Foil	Thickness μm	Mean energy [in MeV]	Energy loss [in MeV]
Pt	12.5	26.48	2.58
Cu	10.0	24.51	1.36
Pt	12.5	22.4	2.85
Cu	10.0	20.19	1.56
Pt	12.5	17.78	3.27
Cu	10.0	15.20	1.89
Pt	12.5	12.24	4.01
Cu	10.0	8.91	2.67

four stacks were irradiated with ^{3}He-particles and three with alphas. A typical composition of the stack, the corresponding mean alpha energies and the alpha energy losses in the foils are given in Table I.

The average particle energy effective at each foil was calculated using the standard formalism [27] and corrected by the method described in [24]. The energy degradation along the stack and the beam current were checked by the reactions induced in the inserted Ti or Cu monitor foils. The reactions used were the following: ^{nat}Ti(^{3}He, x)^{48}V [22], ^{63}Cu(α, n)^{66}Ga [28] and ^{65}Cu($\alpha, 2n$)^{67}Ga [28]. In studies on the ^{197}Au(p, n)^{197}Hg^{m,g} reactions 20μm thick Au foils (99.999%, Goodfellow, England) together with Cu-monitor foils were irradiated in a stack with 20.0 MeV protons. The method of energy calculation was the same as described above and the monitor reactions used were ^{63}Cu(p, n)^{63}Zn [29] and ^{65}Cu(p, n)^{65}Zn [30]. The beam intensity was calculated in every monitor position using all the available monitor reactions and these "currents" were reflected in the primary particle energy incident on the front foil of the stack. The beam current was calculated as the mean of the individually calculated currents, and the primary particle energy was determined to get the minimum χ^2 for the beam current, taking into account the errors of the measured activity and the used cross sections. Besides monitor foils, the charge collected in a Faraday cup was also registered and therefrom the average beam current was deduced. The two results generally agreed within 10%.

TABLE II: Decay data of measured reaction products[a]

Reaction product	Half-life	Mode of decay(%)	E_γ [in keV]	I_γ [in %]
^{48}V	15.97 d	EC(50.4), β^+(49.6)	983.5	99.98
			1312.09	97.48
^{66}Ga	9.49 h	EC(43.5), β^+(56.5)	833.4	5.89
			1039.2	37.0
^{67}Ga	3.26 d	EC(100)	184.5	21.2
			300.2	16.8
^{65}Zn	244.26 d	EC(98.54), β^+(1.46)	1115.5	50.6
$^{195}Hg^m$	1.73 d	IT(54), EC(46)	560.03	7.5
$^{195}Hg^g$	9.9 h	EC(100)	779.77	6.8
$^{197}Hg^m$	23.8 h	IT(93.5), EC(6.5)	133.96	34.1
$^{197}Hg^g$	64.14 h	EC(100)	191.36	0.608
			77.34	18
$^{196}Au^m$	9.7 h	IT(100)	147.81	42.5
$^{196}Au^g$	6.18 d	EC(93.0), β^-(7.0)	355.68	86.9

[a]Taken from Refs. [31, 32].

B. Measurement of radioactivity

A HPGe and a low energy HPGe detector were used to measure the activities of ^{48}V, ^{66}Ga, ^{65}Zn and ^{67}Ga in the irradiated monitor foils and the activities of $^{195}Hg^{m,g}$, $^{197}Hg^{m,g}$ and $^{197}Au^{m,g}$ in the irradiated samples. The energies and branching ratios of the used gamma lines are given in Table II [cf. 31, 32]. The monitor foils were measured by the HPGe detector, while the platinum samples were measured using both the HPGe and low energy HPGe (with thin window) detectors. Peak area analyses were done using the PC version of the GAMANAL [33, 34] spectrum analyser programme.

The detector efficiency was determined experimentally using a selected set of γ-ray standard sources (obtained from Amersham International or PTB, Braunschweig). Corrections were applied for the extended form of samples and for self-absorption. The true coincidence

corections for the gamma lines were calculated by the TrueCoinc code [cf. 35]. The count rate for each gamma line was measured many times as a function of time, and the decay curve analysis was performed in each case. An example of the measured γ-ray spectrum covering the energy range 550 to 800 keV is shown in Fig. 1(a). The analysis of γ-peaks relevant to $^{195}Hg^{m}$ and $^{195}Hg^{g}$ is shown in Fig. 1(b) and (c) and the decay of the peaks in Fig. 1(d). Similar peak analyses were done for the other radionuclides. There was considarable difficulty in measuring the activity of the isotope $^{197}Hg^{g}$ since the intensity of the 191 keV gamma line is very low and the 77 keV line was overlapped by the X-rays of the products. The GAMANAL was able to separate the intensity of the 77 keV γ-line from the X-rays. However ^{197}Pt also produces the same gamma lines, which can be separated only by the decay curve analysis. Unfortunately the half-life of ^{197}Pt (18.3 h) is very close to that of $^{197}Hg^{m}$ (23.8 h), therefore their separation by the fitting method was not reliable. The $^{197}Hg^{m}$ contribution was subtracted based on an independent determination of the activity via the 134 keV γ-line. Finally the $^{197}Hg^{g}$ and $^{197}Pt^{g}$ contributions were separated by fitting the decay curves.

C. Calculation of cross sections, isomeric cross-section ratios and their uncertainties

The count rates at the end of bombardment (EOB) were converted to decay rates A_g, A_m by introducing corrections for emission probabilities of $\gamma-$rays, detector efficiency, self-absorption, coincidence loss, dead time, random pile up, and the size of the beam spot. The decay rates as a function of cooling time (t) after T irradiation time are described in the following equations [cf. 36]:

$$A_m(t) = \lambda_m N_m(t) = \lambda_m \sigma_m n_0 \Phi_{\lambda_m} e^{-\lambda_m t} \tag{6}$$

$$A_g(t) = \lambda_g N_g(t) = \lambda_g \left(\left(\sigma_g + \frac{P_m \lambda_m}{\lambda_m - \lambda_g} \sigma_m \right) n_0 \Phi_{\lambda_g} e^{-\lambda_g t} - \frac{P_m \lambda_m}{\lambda_m - \lambda_g} N_m(T) e^{-\lambda_m t} \right) \tag{7}$$

where

$$\Phi_{\lambda_x} = e^{-\lambda_x T} \int_0^T \phi(t) e^{\lambda_x t} dt \tag{8}$$

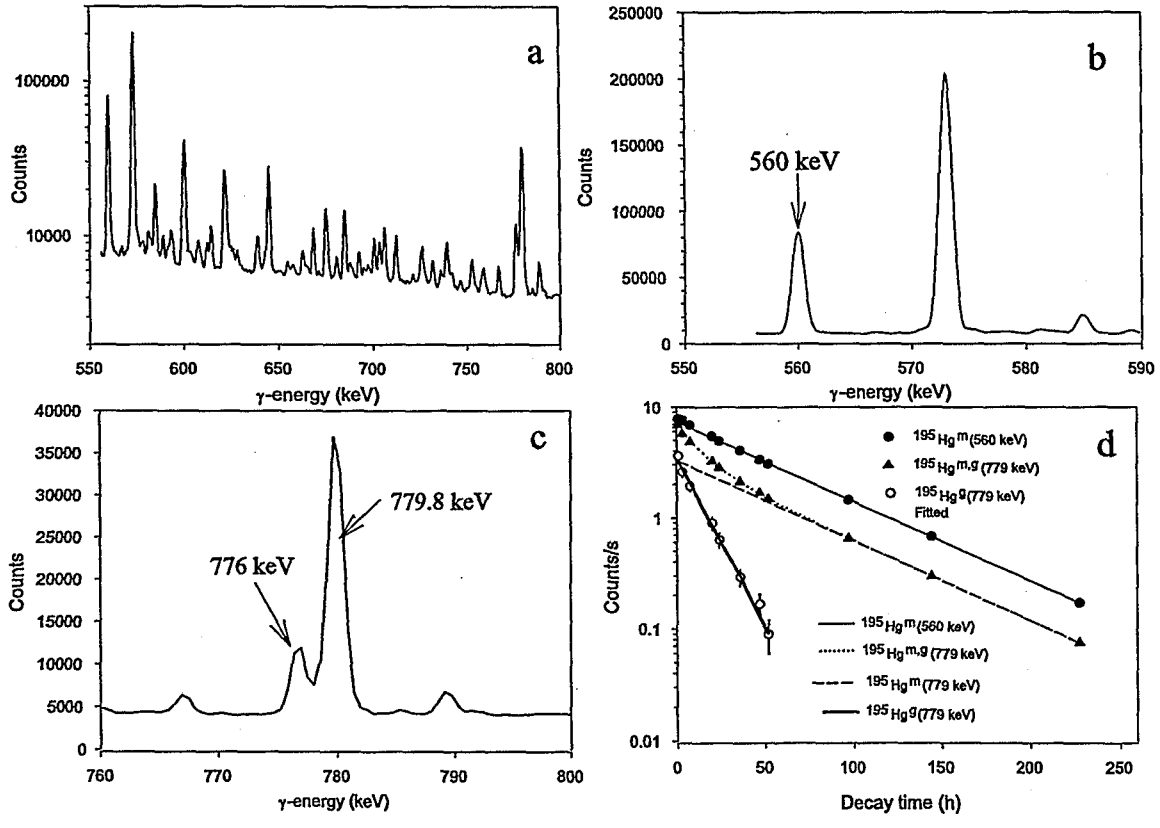

FIG. 1: (a) Measured γ-ray spectrum, (b) the peak at 560 keV of ^{195}Hg^{m}, (c) the peak at 779.8 keV of ^{195}Hg^{m} and ^{195}Hg^{g}, (d) γ-lines and the fitted decay curves. Whereas the decay of the 560 keV γ-ray corresponds purely to ^{195}Hg^{m}, in the case of the 779.8 keV γ-ray two components could be analysed.

In this expression, σ_x, λ_x are production cross section and decay constant for meta ($x = m$) and ground state($x = g$), respectively. P_m is the branching ratio of the metastable state to the ground state, n_0 the number of the target nuclei per cm^2 and $\phi(t)$ is the flux of the incident beam in particles per second. The cross section for the metastable state can be determined directly from Eq. 6. In those cases where the half-lives of the meta and ground states are quite near, the analysis of decay curve of the ground state from Eq. 7 gives only the cumulative cross section of the meta and ground state, i.e. $\sigma_c = \sigma_g + \frac{P_m \lambda_m}{\lambda_m - \lambda_g}\sigma_m$. The σ_g was calculated using the data of σ_c and σ_m.

In cases where both detectors were used for activity measurement, the cross section was deduced as a weighted average of data obtained from independent measurements. The results from the different detectors agreed within the limits of their uncertainties of measurements. The individual uncertainties were combined in quadrature, taking into account the correlation of the data, to obtain an overall uncertainty of $9-31\%$ for the cross sections. The isomeric cross-section ratio was calculated as the ratio of the σ_m and σ_g. The uncertainties in the isomeric cross-section ratios were obtained by combining in quadrature the uncertainties in the individual cross sections involved, taking into account the correlation of the data. In general, the total uncertainty for each ratio was $9-50\%$.

III. NUCLEAR MODEL CALCULATIONS

Cross sections were calculated using the statistical model taking into account the pre-equlibrium effects. In general, two codes, namely STAPRE and EMPIRE, were used.

A. STAPRE calculations

The details of the code are given elsewhere [37]. The transmission coefficients for neutrons, protons, alpha and ^{3}He-particles were provided as input data to the STAPRE code by means of the spherical optical model code SCAT-2[38]. They were generated in SCAT-2 using parameters chosen from a global parameter set. For neutron, the optical model parameter set of Ferrer et al. [39] and for proton that of Perey [40] were used. In the case of alpha particles, a modified set of optical model parameters of McFadden and Satchler [41] was used. The ^{3}He can be treated as input particle, and the potentials of Becchetti and Greenlees [42] were used. The potentials used for neutrons were checked by comparing their predictions of nonelastic and total cross sections with the experimental data[43], wherever available. For the energy (E) and mass (A) dependence of the absolute square of the average effective matrix element of the residual interactions ($|M|^2$, the $|M|^2 = (FM)\cdot A^{-3}E^{-1}$) formula was used [44]. In the present work the emphasis was on the isomeric cross sections. Since such calculations are strongly dependent on the input level scheme of the product nucleus [1, 3], we chose those parameters carefully. The energies, spins, parities and branching ratios of discrete levels were extracted by using the NNDC On-Line Data Service from the ENSDF

database [45]. In cases where the spin and parity were not known, estimates from adjacent levels were made. In the continuum region the level density was calculated by the back-shifted formula and the level density parameter given in Refs. [8, 46]. The level density parameter a for the calculation was selected by interpolating the data of the neighboring isotopes, taking into account the odd-even systematics[46]. The back-shift parameter (Δ) was determined individually for all nuclei used in the model calculation. The cumulative plot of the known discrete levels, collected from the ENSDF database, was fitted by the BSFG formula while the level spacing at the neutron binding energy was kept according to the experimental value. Another important consideration in calculating the isomeric cross sections is the spin distribution of the level density [cf. 1, 4, 47].

We characterized the spin distribution of the level density by the parameter η (see above) and the calculations were performed for different η values to find the best value getting agreement with the experimental data. The transmission coefficients of photons are also of considerable significance in calculations on isomeric cross sections. They were derived from the gamma-ray strength functions. For the E1 transition the Brink-Axel model with global parameters was applied, while for the M1, E2, M2, E3 and M3 radiation the Weisskopf model was used.

B. EMPIRE calculations

In most of the STAPRE calculations done in this work an η value of about 0.25 was found to be most suitable as compared to about 0.5 normally used. In order to check the credibility of those calculations we also used the EMPIRE-II(version 2.19) code [48]. In this case the standard library of input parameters was used which includes the nuclear masses, optical model parameters, ground state deformations, discrete levels and decay schemes, level densities, moments of inertia (MOMFIT), and strength functions. For the proton induced reaction the direct contribution was determined via the Coupled Channel calculation using the built in ECIS03 code. The particle transmission coefficients were generated via the spherical optical model using the computer code (ECIS03) and the default set of global parameters: for neutrons and protons from [49], for alpha particles from [41], and for ^{3}He-particles from [42]. In the calculation the Multi Step Direct, Multi Step Compound, Hauser-Feshbach model with width fluctuation correction (HRTW), the DEGAS and PCROSS codes

were used. These codes conserve the particle flux by dividing the absorption cross section of the optical model between the different types of reaction mechanisms. For the level densities, the dynamic approach of the EMPIRE-II and HF-BCS microscopic level densities were used. In the case of the dynamic approach, the formalism of the super-fluid model (BCS) was applied below the critical excitation energies and the Fermi gas model above the critical energy.

IV. RESULTS AND DISCUSSION

A. Cross sections and excitation functions

The reaction cross sections determined through identification of the activation products via γ−ray spectrometry are given in Tables III, IV and V. For some data points the calculated uncertainty was too large; therefore they are not presented. We discuss below the data for each individual reaction in some detail.

The excitation functions of the ^{nat}Pt(^{3}He, xn)^{195}Hg^{m,g} reactions are given in Figures 2 and 3. Considering the Q-values of the reactions and the isotopic composition of natural platinum, the major contributing reactions appear to be: ^{194}Pt(^{3}He, $2n$)^{195}Hg^{m,g}, ^{195}Pt(^{3}He, $3n$)^{195}Hg^{m,g} and ^{196}Pt(^{3}He, $4n$)^{195}Hg^{m,g} processes. The direct reaction process would involve the stripping of two protons, which would need the radioactive ^{193}Pt target nucleus. Therefore, the processes should go through compound and precompound ways. The experimental data and the results of nuclear model calculations were normalised according to the abundances of the contributing Pt isotopes. The averaged experimental data are in good agreement with the results of nuclear model calculations.

The excitation functions of the ^{nat}Pt(^{3}He, xn)^{197}Hg^{m,g} reactions are given in Figures 4 and 5. Based on considerations discussed above, the contributing processes should be: ^{194}Pt(^{3}He, γ)^{197}Hg^{m,g}, ^{195}Pt(^{3}He, n)^{197}Hg^{m,g}, ^{196}Pt(^{3}He, $2n$)^{197}Hg^{m,g} and ^{198}Pt(^{3}He, $4n$)^{197}Hg^{m,g}. The major part of the cross section for the formation of ^{197}Hg^{m,g} is thus probably constituted by the (^{3}He, $2n$) and (^{3}He, $4n$) processes. The experimental data appear to be in good agreement with the model calculation, both for ^{197}Hg^m and ^{197}Hg^g. The direct reaction process would involve two proton stripping, which could occur on ^{195}Pt target nucleus. Therefore the cross sections may include some contribution from

TABLE III: Activation cross sections of ^{3}He-particle induced reactions on Pt producing Hg isotopes

	^{nat}Pt(^{3}He, xn)^{195}Hg^{m,g}			^{nat}Pt($^{3}He, xn$)^{197}Hg^{m,g}		
$<E_{^3He}>^a$	^{195}Hg^{m}	^{195}Hg^{g}	ratio	^{197}Hg^{m}	^{197}Hg^{g}	ratio
(MeV)	mb	mb		mb	mb	
18.07 ± 0.28	3.25 ± 0.20	3.67 ± 0.16	0.89 ± 0.07	0.30 ± 0.03	0.74 ± 0.23	0.41 ± 0.06
18.16 ± 0.27	1.82 ± 0.14	1.90 ± 0.12	0.96 ± 0.10	0.21 ± 0.02		
18.65 ± 0.23	2.72 ± 0.20	2.90 ± 0.19	0.94 ± 0.09	0.27 ± 0.03	6.48 ± 4.74	0.04 ± 0.03
21.50 ± 0.23	29.20 ± 1.55	25.74 ± 1.31	1.13 ± 0.08	2.30 ± 0.19	13.41 ± 1.20	0.17 ± 0.03
21.59 ± 0.22	27.48 ± 2.02	23.50 ± 1.72	1.17 ± 0.12	1.83 ± 0.21	7.39 ± 3.29	0.25 ± 0.11
22.22 ± 0.22	32.36 ± 2.40	28.35 ± 1.67	1.14 ± 0.11	2.45 ± 0.28		
24.61 ± 0.21	85.06 ± 4.44	58.75 ± 3.16	1.45 ± 0.11	11.65 ± 0.94	28.47 ± 3.56	0.41 ± 0.06
24.70 ± 0.21	84.26 ± 6.20	50.56 ± 4.52	1.67 ± 0.19	10.27 ± 1.17	15.74 ± 4.36	0.65 ± 0.20
25.45 ± 0.20	93.69 ± 6.91	54.97 ± 3.19	1.70 ± 0.16	13.15 ± 1.50		
26.71 ± 0.20	121.83 ± 8.96	61.00 ± 3.82	2.00 ± 0.19	23.23 ± 2.65	17.87 ± 6.64	1.30 ± 0.51
27.57 ± 0.18	138.49 ± 10.21	70.24 ± 4.12	1.97 ± 0.19	25.39 ± 2.90	26.06 ± 10.53	0.97 ± 0.41
28.43 ± 0.18	141.61 ± 10.43	69.11 ± 3.95	2.05 ± 0.19	28.24 ± 3.22	24.16 ± 10.31	1.17 ± 0.37
29.60 ± 0.17	158.44 ± 11.66	68.01 ± 4.11	2.33 ± 0.22	35.21 ± 4.02		
30.25 ± 0.17	177.92 ± 13.10	79.58 ± 4.56	2.24 ± 0.21	37.67 ± 4.30		
31.91 ± 0.16	178.39 ± 9.43	62.08 ± 2.27	2.87 ± 0.18	34.40 ± 2.78	54.27 ± 6.79	0.63 ± 0.09
32.31 ± 0.16	172.14 ± 12.65	62.29 ± 3.44	2.76 ± 0.25	32.45 ± 3.70	16.77 ± 8.86	1.93 ± 1.05
33.74 ± 0.15	191.40 ± 10.11	70.09 ± 2.56	2.73 ± 0.18	31.17 ± 2.52	62.02 ± 7.13	0.50 ± 0.07
34.87 ± 0.15	162.01 ± 11.91	53.35 ± 3.66	3.04 ± 0.31	25.00 ± 2.86	45.47 ± 11.62	0.55 ± 0.15

[a]The uncertainty of the mean energy for the foil

direct interactions besides compound and precompound processes. The contribution of the ^{195}Pt(^{3}He, n)^{197}Hg^{m,g} process in the compound and preequilibrium reaction is less than 5 percent of the total compound and precompound cross section.

The excitation functions of the ^{nat}Pt(^{3}He, x)^{196}Au^{m,g} reactions are given in Figures 6 and 7. The contributing processes are ^{194}Pt(^{3}He, p)^{196}Au^{m,g}, ^{195}Pt(^{3}He, $pn+d$)^{196}Au^{m,g} and ^{196}Pt(^{3}He, $p2n+dn+t$)^{196}Au^{m,g}. Presumably, in the one proton stripping process on ^{195}Pt

TABLE IV: Activation cross sections of ^{3}He-particle induced reactions on Pt producing $^{196}Au^{m,g}$

	$^{nat}Pt(^{3}He, pxn)^{196}Au^{m,g}$		
$<E_{^3He}>^a$	$^{196}Au^m$	$^{196}Au^g$	ratio
(MeV)	mb	mb	
18.07 ± 0.28	0.05 ± 0.01	6.21 ± 0.02	0.007 ± 0.001
18.16 ± 0.27		3.32 ± 0.07	
18.65 ± 0.23	0.05 ± 0.01	4.73 ± 0.03	0.011 ± 0.002
21.5 ± 0.23	0.51 ± 0.06	35.47 ± 0.08	0.014 ± 0.002
21.59 ± 0.22	0.36 ± 0.04	29.51 ± 0.08	0.012 ± 0.001
22.22 ± 0.22	0.46 ± 0.06	37.59 ± 0.18	0.012 ± 0.002
24.61 ± 0.21	1.62 ± 0.19	69.38 ± 0.22	0.023 ± 0.003
24.7 ± 0.21	1.46 ± 0.17	64.80 ± 0.20	0.023 ± 0.003
25.45 ± 0.2	1.97 ± 0.23	78.07 ± 0.40	0.025 ± 0.003
26.71 ± 0.2	3.87 ± 0.44	88.46 ± 0.49	0.044 ± 0.005
27.57 ± 0.18	4.01 ± 0.46	103.52 ± 0.55	0.039 ± 0.004
28.43 ± 0.18	4.41 ± 0.50	103.73 ± 0.64	0.043 ± 0.005
29.6 ± 0.17	6.69 ± 0.75	101.99 ± 0.84	0.066 ± 0.007
30.25 ± 0.17	6.83 ± 0.77	118.08 ± 0.86	0.058 ± 0.007
31.91 ± 0.16	7.81 ± 0.89	107.68 ± 0.99	0.072 ± 0.008
32.31 ± 0.16	8.96 ± 1.01	97.17 ± 1.10	0.092 ± 0.010
33.74 ± 0.15	8.79 ± 1.03	106.52 ± 1.15	0.083 ± 0.010
34.87 ± 0.15	9.55 ± 1.08	82.52 ± 1.68	0.116 ± 0.013

[a]The uncertainty of the mean energy for the foil

strong direct interactions are involved. The results of nuclear model calculations for both the m and g states give too low values, supporting the assumption of occurrence of direct interactions.

The excitation functions of the $^{nat}Pt(\alpha,xn)^{197}Hg^{m,g}$ reactions are given in Figures 8 and 9. The major contributing processes should be $^{194}Pt(\alpha,n)^{197}Hg^{m,g}$ and $^{195}Pt(\alpha,2n)^{197}Hg^{m,g}$. The results of nuclear model calculations agree fairly well both for the formation of the

TABLE V: Activation cross sections of α-particle induced reactions on Pt producing $^{197}Hg^{m,g}$

	$^{nat}Pt(\alpha, xn)^{197}Hg^{m,g}$		
$<E_\alpha>^a$	$^{197}Hg^m$	$^{197}Hg^g$	ratio
(MeV)	mb	mb	
16.2 ± 0.30	0.16 ± 0.01		
17.8 ± 0.26	3.6 ± 0.3	9.3 ± 2.7	0.38 ± 0.12
19.5 ± 0.25	11.6 ± 0.9	22 ± 2	0.53 ± 0.07
21.2 ± 0.23	35 ± 3	50 ± 5	0.70 ± 0.09
22.4 ± 0.22	73 ± 6	83 ± 12	0.88 ± 0.14
24.0 ± 0.20	107 ± 9	99 ± 15	1.08 ± 0.19
25.6 ± 0.18	158 ± 13	121 ± 22	1.30 ± 0.25
26.5 ± 0.15	181 ± 15	111 ± 23	1.63 ± 0.37

[a]The uncertainty of the mean energy for the foil

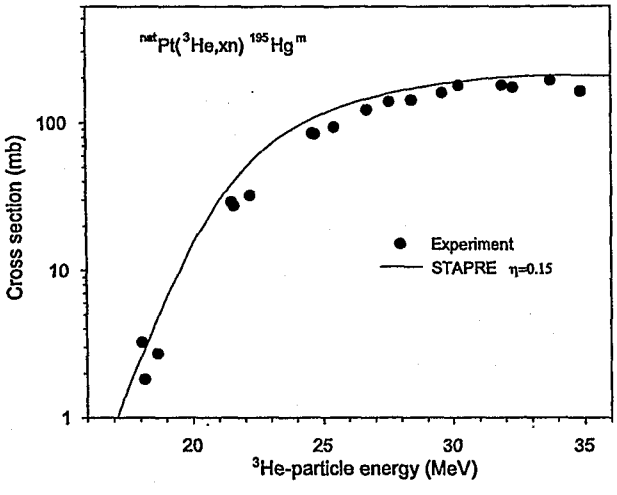

FIG. 2: Excitation function of the $^{nat}Pt(^3He, xn)^{195}Hg^m$ reaction.

ground state and the metastable state, suggesting that the statistical processes play a dominant role. The direct process could be the two proton stripping on ^{195}Pt, which, however appears to be rather weak.

For the reactions $^{197}Au(p, n)^{197}Hg^{m,g}$ we did not measure the individual excitation func-

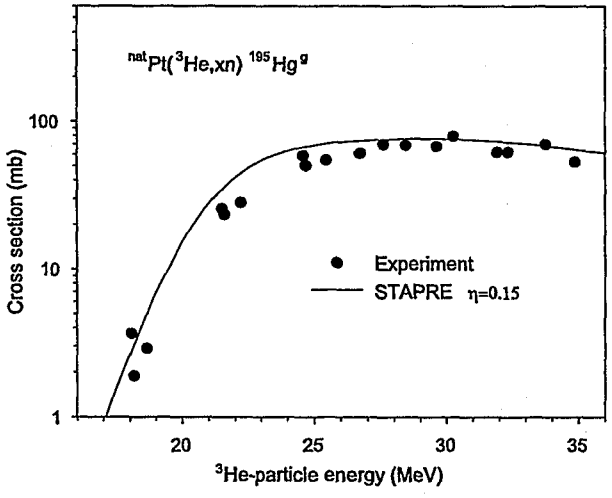

FIG. 3: Excitation function of the ^{nat}Pt(^{3}He, xn)^{195}Hg^g reaction.

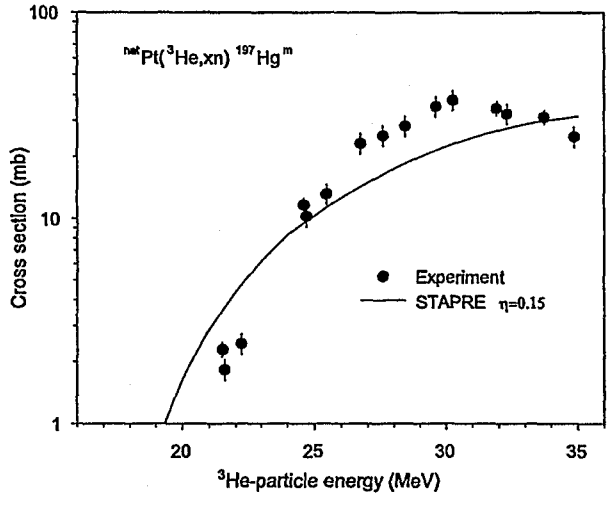

FIG. 4: Excitation function of the ^{nat}Pt(^{3}He, xn)^{197}Hg^m reaction.

tions; only the isomeric cross-section ratios were determined and the results are given in Table VI.

B. Isomeric cross-section ratios

The isomeric cross-section ratio (σ_m/σ_g) for the pair ^{195}Hg^{m,g} in ^{3}He-particle induced reactions on ^{nat}Pt is shown in Figure 10 as a function of energy. The ratio increases from a value of about 1 at 18 MeV to a value of about 3.3 at 35 MeV, i.e. the higher spin isomer is

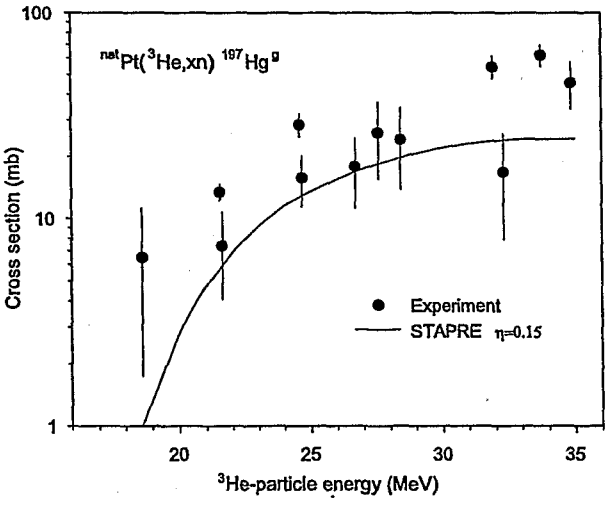

FIG. 5: Excitation function of the ^{nat}Pt(^{3}He, xn)^{197}Hg^{g} reaction.

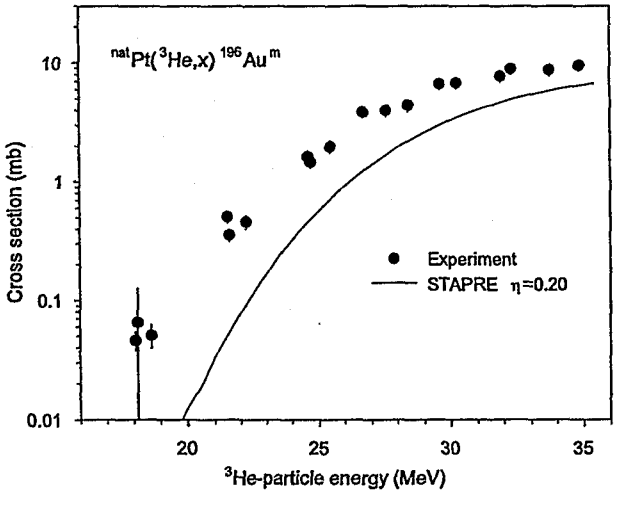

FIG. 6: Excitation function of the ^{nat}Pt(^{3}He, x)^{196}Au^{m} reaction.

strongly favoured at higher energies. The results of nuclear model calculations using the code STAPRE as well as EMPIRE II are also shown. In the former case, four η values ranging between 0.15 and 0.25 were chosen and the results are shown for two values. The EMPIRE II could not reproduce the experimental data, and STAPRE gave values comparable to the experimental data only when an η value of 0.15 was adopted.

Similar to ^{195}Hg^{m,g} the isomeric cross-section ratios for the pairs ^{197}Hg^{m,g} and ^{196}Au^{m,g} in ^{3}He-particle induced reactions on ^{nat}Pt are shown in Figures 11 and 12, respectively, as

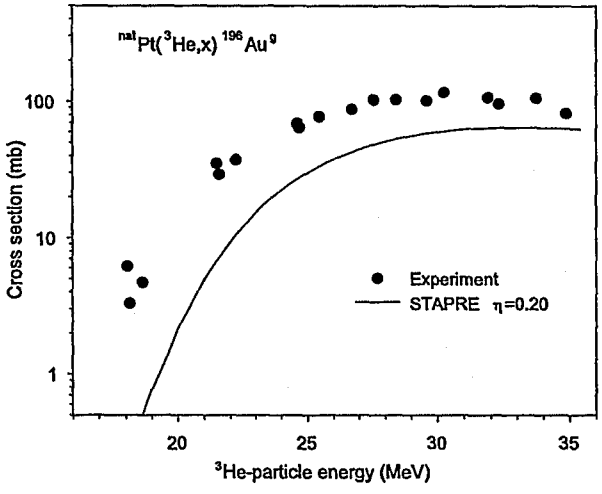

FIG. 7: Excitation function of the ^{nat}Pt(^{3}He, x)^{196}Au^g reaction.

TABLE VI: Isomeric cross-section ratios for the ^{197}Au$(p,n)^{197}$Hg^{m,g} reactions

$<E_p>^a$ (MeV)	ratio
8.8 ± 0.3	0.26 ± 0.03
11.2 ± 0.3	0.47 ± 0.08
13.2 ± 0.2	0.58 ± 0.09
15.0 ± 0.2	0.61 ± 0.05
16.7 ± 0.2	0.72 ± 0.06
18.3 ± 0.2	0.93 ± 0.06

[a]The uncertainty of the mean energy for the foil

a function of energy. In the case of ^{197}Hg^{m,g} (Fig. 11), the ratio varies between 0.5 and 1.0. It is reproduced well by the STAPRE calculation using an η value of 0.15; the EMPIRE II calculation gives a completely different magnitude and trend. For ^{196}Au^{m,g} (Fig. 12) the ratio is very low, presumably due to the very high spin of the metastable state, but the trends are similar: the experimental ratio increases with the ^{3}He-particle energy from a very low value at 18 MeV to about 0.1 at 35 MeV, the STAPRE calculation reproduces the data when an η value of 0.25 is used, and strong deviations are observed when either EMPIRE

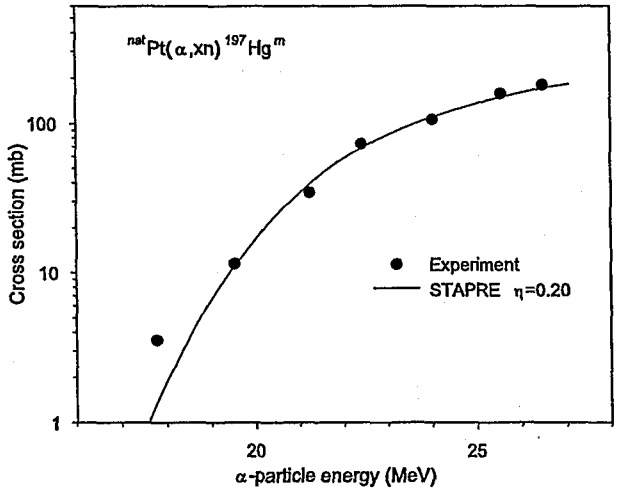

FIG. 8: Excitation function of the $^{nat}\mathrm{Pt}(\alpha, xn)^{197}\mathrm{Hg}^{m}$ reaction.

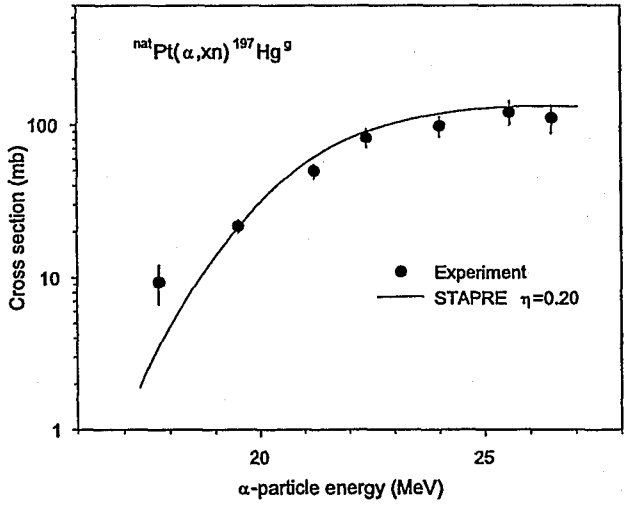

FIG. 9: Excitation function of the $^{nat}\mathrm{Pt}(\alpha, xn)^{197}\mathrm{Hg}^{g}$ reaction.

II code is used or when STAPRE calculation uses an η value of 0.5.

The isomeric cross-section ratio for the pair $^{197}\mathrm{Hg}^{m,g}$ in α-particle induced reactions on ^{nat}Pt is shown in Figure 13. The value is about 0.5 near the thresholds of the two reactions, increasing to about 1.8 at 26 MeV. Our data agree with the results of Vandenbosch and Huizenga [17]. The STAPRE calculation reproduces the ratio well when an η value between 0.15 and 0.25 is used. As in other cases, the EMPIRE II does not reproduce the ratio above 20 MeV.

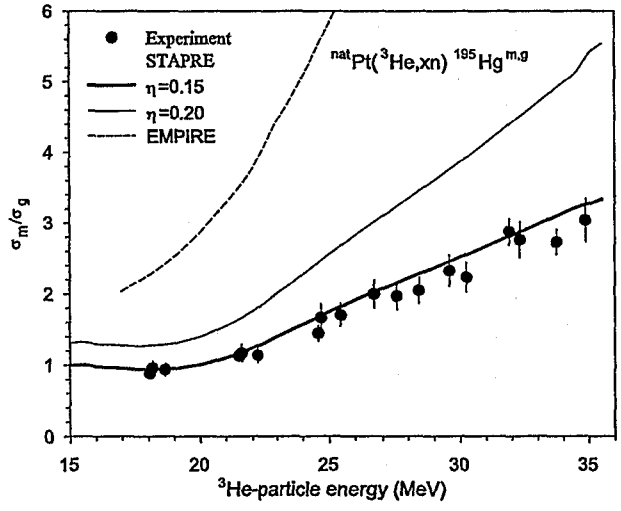

FIG. 10: Isomer ratio in the ^{nat}Pt(^{3}He, xn)^{195}Hg^{m,g} process.

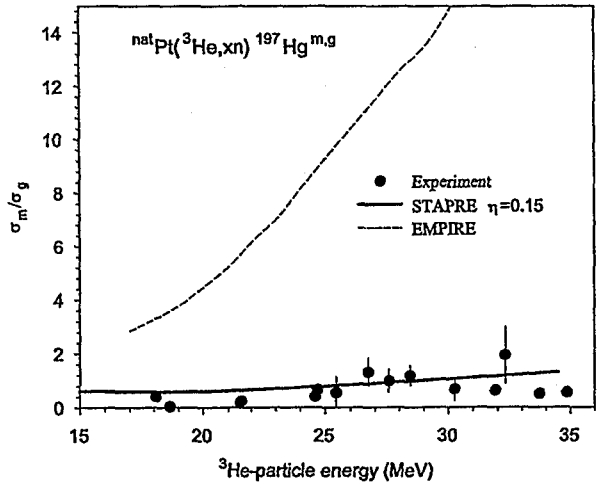

FIG. 11: Isomer ratio in the ^{nat}Pt(^{3}He, xn)^{197}Hg^{m,g} process.

The isomeric cross-section ratio for the pair ^{197}Hg^{m,g} in proton induced reactions on ^{197}Au is shown in Figure 14. As mentioned above, this ratio was measured earlier by several groups [17–21] and the results above 10 MeV are conflicting. A detailed analysis shows that in some cases the true coincidence corrections were omitted in the evaluation of the experimental data and the authors used small distance between the detector and sample. In one case [21], based on the presented gamma ray spectrum, we could calculate the true coincidence corrections (approximately) and the Fig. 14 shows only those experiments where

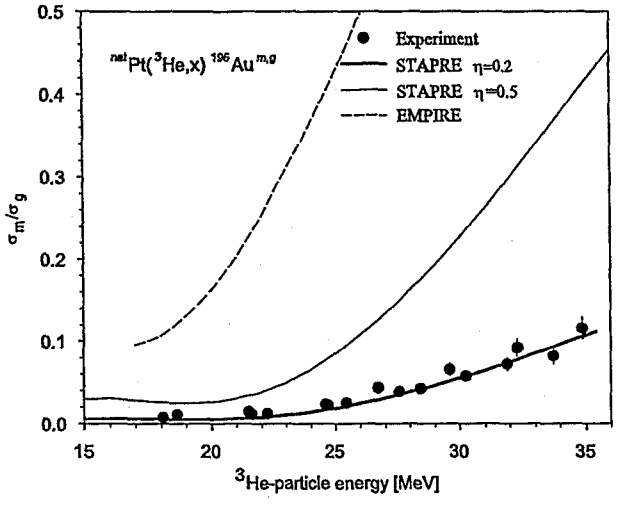

FIG. 12: Isomer ratio in the ^{nat}Pt(^{3}He, x)^{196}Au^{m,g} process.

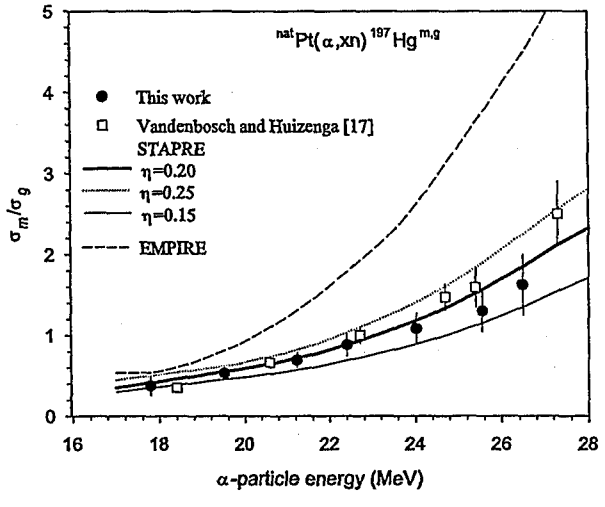

FIG. 13: Isomer ratio in the ^{nat}Pt(α, xn)^{197}Hg^{m,g} process.

the coincidence corrections were applied. Our experimental data are also given; they are in agreement with the lower values and appear to be reproduced well by the STAPRE calculation using an η value of about 0.25. The sensitivity of the calculation is shown by the large deviation of the calculated data with $\eta = 0.5$. The figure also shows the model calculations with the EMPIRE 2.19. The dotted line gives the results of the EMPIRE calculation using the dynamic approach for the level density, while the dashed line shows the calculations using the HF-BCS microscopic model based level density. Both calculations

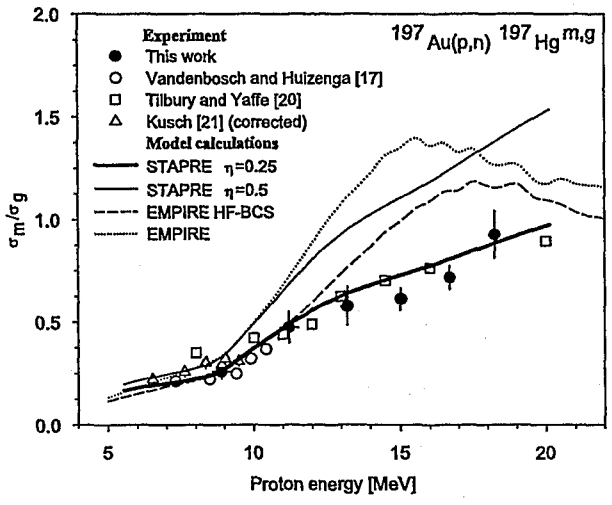

FIG. 14: Isomer ratio in the $^{197}\mathrm{Au}(p,n)^{197}\mathrm{Hg}^{m,g}$ process.

take into account the direct processes by the ECIS03 coupled channel code. The exciton model part of the EMPIRE, DEGAS uses its own spin-cutoff parameter for the momentum distribution. It includes charge exchange process in the calculation. It can be seen in Fig. 14 that EMPIRE with the dynamic approach even more overestimates the isomeric cross-section ratio than the STAPRE with $\eta = 0.5$. The EMPIRE result with the HF-BCS microscopic level density agrees up to 11 MeV very well with the experimental data and the STAPRE calculation with $\eta = 0.25$ value. Above this energy, when the preequilibrium emission, calculated by DEGAS, becomes more important, the deviation between the two models (and the experiment) increases. This deviation can be explained on the basis that the DEGAS uses an independent momentum distribution of the levels.

V. CONCLUSION

Experimental and theoretical studies show that the excitation functions of ^{3}He- and α-particle induced reactions on ^{nat}Pt leading to the formation of the isomeric pairs $^{195}\mathrm{Hg}^{m,g}$ and $^{197}\mathrm{Hg}^{m,g}$ are described well by the statistical theory incorporating pre-compound effects. The formation of the pair $^{196}\mathrm{Au}^{m,g}$, on the other hand, appears to entail strong direct interactions. Despite the relatively high spins of the metastable states, the isomeric cross-section ratios are relatively high for the pairs $^{195}\mathrm{Hg}^{m,g}$ and $^{197}\mathrm{Hg}^{m,g}$ even at low excitation energies; they

increase with the increasing projectile energy. The ratio is very small for the pair $^{196}Au^{m,g}$, presumably due to the high spin (12^-) of the metastable state. The isomeric cross-section ratio for each of the three pairs appears to be reproduced by the STAPRE calculation only when an η value of 0.25 or less is used. Our measured isomeric cross-section ratios confirm some of the earlier experiments. The ratios cannot be described by a nuclear reaction model code using the conventional level density formalism with the usual η value. The agreement between the STAPRE calculation with $\eta = 0.25$ and EMPIRE with HF-BCS microscopic treatment implies that the low η values originate from the microscopic structure of these nuclei.

The advantage of using the alpha and helium-3 induced reactions for studying the isomeric cross-section ratio is that the compound system gets larger angular momentum transferred than in nucleon induced reactions. As a result the isomeric cross-section ratio becomes more sensitive to the spin distribution. The energy dependence of the isomeric cross-section ratio is described well by the model calulations. This implies that the contribution of two proton stripping direct process is negligible. It also indicates that to a first approximation η is independent of energy and the energy dependence of the spin-cutoff factor is adequate.

A further support to the present results is furnished by our new measurements on the $^{196}Hg(n,2n)^{197}Hg^{m,g}$ process [50]. An analysis of that measurement confirmed the low value of η. In that case obviously proton stripping does not play any role.

The characteristics of the discrete levels as well as their branching ratios play an important role in the calculation of isomeric cross-section ratios. The constancy in the η value in describing (within the uncertainty of the experimental data) the different particle induced reactions (α, ^{3}He, p, n) shows that there cannot be any serious error in the decay scheme of the discrete levels. Since the population of the discrete levels by particle emission and gamma cascade from the continuum will be different for different types of reactions, the error in the level scheme would lead to a large deviation between the needed η values to fit the calculated and measured isomeric cross-section ratios. For example the maximum of the spin distribution for the ^{198}Hg compound nucleus is at 5 $\hbar$ in the $^{197}Au(p,n)^{197}Hg^{m,g}$ reaction but it is at 16 $\hbar$ in the $^{194}Pt(\alpha,n)^{197}Hg^{m,g}$ reaction at about the same excitation energy of the ^{198}Hg. It can thus be stated that the spin-cutoff factor and the ratio of the effective moment of inertia Θ_{eff} to the rigid-body moment of inertia $\Theta_{rig}(\eta = \Theta_{eff}/\Theta_{rig})$ show anomaly for the isotopes^{195}Hg and ^{197}Hg.

In a recent work [51] the spin cutoff factor (σ) has been evaluated at low excitation energy in the mass range of 20≤A≤110. It was concluded, that using the formula

$$\sigma = const(U - \Delta)^{0.25} A^{5/6}/a^{1/4}, \tag{9}$$

for the energy(U), energy shift(Δ), mass number(A) and level density parameter(a) dependence of σ, the fitted "const" in the formula shows a mass number dependence.

$$const = 0.10578 - 0.000202A. \tag{10}$$

This "const" is directly connected to the parameter η used in this paper:

$$\eta^{1/2} = \frac{const}{const_{rig}} = 0.878152 - 0.001677A \tag{11}$$

If we accept the mass dependence given above the extrapolated value for the η(197)=0.30, which is quite near to our value of 0.25 from the isomeric cross-section measurement. It can also be seen from the evaluation of [51], that the individual values strongly scattered around the value in equation 10.

The recent analysis of Ref. [52] suggesting $\eta = 0.75$ for ^{51}V, a lot of successful model calculations with $\eta = 0.5$ in the medium mass region, and our conclusion of $\eta = 0.25$ for heavy nuclei, all agree quite well with the data calculated from Eq. 11 (η(51)=0.63, η(100)=0.50,η(197)=0.30,). Since energy dependence for η has not been observed, the results of the low energy analysis can be extended to higher excitation energies and we can postulate that η has a mass dependence even upto mass number 197. These empirical results should be confirmed for the higher mass number region with new experiments, and an explanation of mass dependence needs further theoretical work.

Acknowledgments

We thank Prof. H.H.Coenen and Prof. J.Csikai for their kind support of this project, Mr. S. Spellerberg for some technical assistance and the crew of the compact cyclotron CV 28 at Jülich for performing irradiations.

---

[1] S. M. Qaim, A. Mushtaq, and M. Uhl, Phys Rev. C 38, 645 (1988).

[2] F. Cserpák, S. Sudár, J. Csikai, and S. M. Qaim, Phys Rev. C **49**, 1525 (1994).

[3] S. Sudár and S. M. Qaim, Phys Rev. C **53**, 2885 (1996).

[4] B. Strohmaier, M. Fassbender, and S. M. Qaim, Phys Rev. C **56**, 2654 (1997).

[5] S. Sudár, A. Hohn, and S. M. Qaim, Appl. Radiat. Isot **52**, 937 (2000).

[6] C. D. Nesaraja, S. Sudár, and S. M. Qaim, Phys. Rev. C **68**, 024603 (2003).

[7] H. Bethe, Phys. Rev. **50**, 332 (1936).

[8] W. Dilg, W. Schantl, H. Vonach, and M. Uhl, Nucl. Phys. A **217**, 269 (1973).

[9] S. Hilaire, J. P. Delaroche, and M. Girod, J. Eur. Phys. A **12**, 169 (2001).

[10] P. Demetriou and S. Goriely, Nucl. Phys. A **695**, 95 (2001).

[11] V. Paar, D. K. Sunko, S. Brant, M. G. Mustafa, and R. G. Lanier, Z. Phys. A **345**, 343 (1993).

[12] P. Quentin, H. Lafchiev, D. Samsoen, and I. N. Mikhailov, Phys. Rev. C **69**, 054315 (2004).

[13] B. K. Agrawal, S. K. Samaddar, A. Ansari, and J. N.De, Phys. Rev. C **59**, 3109 (1999).

[14] W. F. Mueller, W. Reviol, M. P. Carpenter, R. V. F. Janssens, F. G. Kondev, and et al, Phys. Rev. C **69**, 064315 (2004).

[15] P. A. DeYoung, B. Atallah, B. Hughey, P. L. Jolivette, M. Kern, G. F. Peaslee, and et. al, Phys. Rev. C **62**, 047601 (2000).

[16] Nuclear Data Centers Network, *Experimental Nuclear Reaction Database (EXFOR)* (International Energy Agency, Vienna, 2004).

[17] R. Vandenbosch and J. Huizenga, Phys. Rev. **120**, 1313 (1960).

[18] L. Hansen, Nucl. Phys. **30**, 389 (1962).

[19] V. Gritsyna, J. Exp. Theo. Phys. (in Russian) **44**, 1770 (1963).

[20] R. Tilbury and L. Yaffe, Can. J. Chem. **41**, 2643 (1963).

[21] W. Kusch, Acta Physica Polonica **B6**, 741 (1975).

[22] R. Weinreich, H. J. Probst, and S. M. Qaim, International J. Applied Radiation Isotopes **31**, 223 (1980).

[23] H. Piel, S. M. Qaim, and G. Stöcklin, Radiochim. Acta **57**, 1 (1992).

[24] S. Sudár and S. M. Qaim, Phys Rev. C **50**, 2408 (1994).

[25] S. Sudár, F. Cserpák, and S. Qaim, Appl. Radiat. Isot. **56**, 821 (2002).

[26] Z. Kormány, Nucl. Instr. Methods Phys. Rea. Section A **337**, 258 (1994).

[27] C. F. Williamson, J. Boujot, and J. Picard, *Tables of Range and Stopping Power of Chemical Elements for Charged Particles of Energy 0.5 to 500 MeV*, Centre d'Etudes de Bruyères-le

Châtel (1966).

[28] E. Bryant, D. Cochran, and J. Knight, Phys. Rev. **130**, 1512 (1963).

[29] R. Collé, R. Kishore, and J. B. Cumming, Phys. Rev. C **9**, 1819 (1974).

[30] P. Kopecky, Appl. Radiat. Isot. **36**, 657 (1985).

[31] E. Browne and R. B. Firestone, *Table of Radioactive Isotopes* (John Wiley and Sons, New York, 1986).

[32] R. B. Firestone, *Table of Isotopes* (John Wiley and Sons, New York, 1996).

[33] R. Gunnink and J. Niday, *Computerized quntitative analysis by gamma-ray spectrometry, Vol. I. Description of the GAMANAL program, UCRL-51061 Vol. 1*, Lawrence Livermore Laboratory (1972).

[34] S. Nagy, *GAMANAL XT/AT user's manual Version 1.1, December 1989 (unpublished)*, Institute of Experimental Physics, Kossuth University, Debrecen, Hungary (1989).

[35] S. Sudár, *TrueCoinc, a software utility for calculation of the true coincidence correction, Specialized software utilities for gamma spectrometry, IAEA-TECDOC-1275*, International Atomic Energy Agency, Vienna (2002).

[36] M. Cavinato, E. Fabrici, E. Gadioli, E. GadioliErba, P. Vergani, M. Crippa, G. Colombo, I. Redaelli, and M. Ripamonti, Phys. Rev. C **52**, 2577 (1995).

[37] M. Uhl and B. Strohmaier, *Computer Code for Particle Induced Activation Cross Section and related Quantities*, Institut für Radiumforschung und Kernphysik, Vienna (1976).

[38] O. Bersillon, *Un programme de modele optique spherique*, Centre d'Etudes de Bruyères-le Châtel (1981).

[39] J. C. Ferrer, J. D. Carlson, and J. Rapaport, Nucl. Phys. A **275**, 325 (1977).

[40] F. G. Perey, Phys. Rev. **131**, 745 (1962).

[41] L. McFadden and G. R. Satchler, Nucl. Phys. **84**, 177 (1966).

[42] F. D. Becchetti and G. W. Greenlees, Phys. Rev. **182**, 1190 (1969).

[43] V. McLane, C. L. Dunford, and P. F. Rose, *Neutron Cross Sections*, vol. 2 (Academic Press, New York, 1988).

[44] C. Kalbach-Cline, Nucl. Phys. **A 210**, 590 (1973).

[45] M. R. Bhat, in *Proceedings of the International Conference on Nuclear Data for Science and Technology*, edited by S. M. Qaim (Springer-Verlag, Berlin, Germany, 1992), p. 817.

[46] V. Plyaskin and R. Kosilov, INDC(CCP)-424 L0 p. 27 (2000).

[47] S. Sudár, F. Szelecsényi, and S. M. Qaim, Phys Rev. C **48**, 3115 (1993).

[48] M. Herman, R. Capote, B. Carlson, P. Oblozinsky, M. Sin, A. Trakov, and V. Zerkin, *EMPIRE-II, Nuclear reaction model code*, International Atomic Energy Agency, version 2.19 (2005).

[49] A. Koning and J. Delaroche, Nuclear Physics A **713**, 231 (2003).

[50] M. Al-Abyad, S. Sudár, M. N. H. Comsan, and S. M. Qaim, Phys. Rev. C, **submitted** (2005).

[51] S. I. Al-Quraishi, S. M. Grimes, T. N. Massey, and D. A. Resler, Phys. Rev. C **67**, 015803 (2003).

[52] V. Avrigeanu, T. Glodariu, A. Plompen, and H. Weigmann, J. Nuclear Science and Technology **Suplement 2**, 746 (2002).